J. Plasma Physics (2009), *vol.* 75, *part* 6, *pp.* 749–768.
doi:10.1017/S002237780900796X

High yield fusion in a staged Z-pinch

H. U. RAHMAN[1], F. J. WESSEL[1], N. ROSTOKER[1]
and P. H. NEY[2]

[1]Department of Physics and Astronomy, University of California, Irvine, CA 92697, USA
[2]Mount San Jacinto College, Menifee, CA 92584, USA
(pney@msjc.edu)

(Received 20 December 2008 and accepted 23 February 2009, first published online 22 April 2009)

Abstract. We simulate fusion in a Z-pinch, where the load is a xenon-plasma liner imploding onto a deuterium–tritium (DT) plasma target and the driver is a 2 MJ, 17 MA, 95 ns risetime pulser. The implosion system is modeled using the dynamic, $2\frac{1}{2}$D, radiation-magnetohydrodynamic code, MACH2. During implosion a shock forms in the Xe liner, transporting current and energy radially inward. After collision with the DT, a secondary shock forms pre-heating the DT to several hundred electronvolts. Adiabatic compression leads subsequently to a fusion burn, as the target is surrounded by a flux-compressed, intense, azimuthal-magnetic field. The intense-magnetic field confines fusion α-particles, providing an additional source of ion heating that leads to target ignition. The target remains stable up to the time of ignition. Predictions are for a neutron yield of 3.0×10^{19} and a thermonuclear energy of 84 MJ, that is, 42 times greater than the initial, capacitor-stored energy.

1. Introduction

The simple Z-pinch is a cylindrical plasma column that implodes to the axis of symmetry when subjected to a large, sustained current pulse. A typical Z-pinch load is constructed from a wire array, foil, plasma jet, or gas-puff, or combinations thereof. When driven by a modern, low-inductance, high-voltage, pulse power circuit, the pinch current pulse can reach many mega-amperes and the delivered power 100s of terawatts. Z-pinch plasmas with keV temperatures and near-solid densities are produced routinely. The Z Facility at the Sandia National Laboratory is perhaps the best example: it produces a 20 MA, 100 ns rise time, 100 TW current pulse and a Z-pinch that can radiate mega-joules of X-ray energy in a pulse of a few nanoseconds. Such plasmas are of great scientific and technical interest, for example in studies related to fusion, atomic physics, laboratory astrophysics, etc. (Matzen 1997; Haines et al. 2000; Ryutov et al. 2000; Coverdale et al. 2007).

The Z-pinch dynamics consists of three phases: implosion, stagnation, and disassembly. The implosion phase is when the discharge current builds and the pinch is driven radially inward by the $\mathbf{J}_z \times \mathbf{B}_\theta$ force, where $\mathbf{J}_z$ is the axial, plasma current density and $\mathbf{B}_\theta$ is the azimuthal, self-magnetic field. At stagnation the pinch is confined briefly, typically for a few nanoseconds when the radial motion of the pinch has ceased, or nearly so, and the plasma is compressed to a high energy density. Generally, the imploded mass and the initial-pinch radius are adjusted so that stagnation occurs after the current maximum.

At stagnation the implosion kinetic energy and the inductive energy, stored local to the pinch, are rapidly converted into plasma internal energy. Shock heating is important. The small radius of the pinch plasma at stagnation also increases its electrical resistance, enhancing the energy deposited by Ohmic heating. Magneto-hydrodynamic (MHD) instabilities occur in this phase: typically, for example the ($m = 0$) sausage instability or the ($m = 1$) kink instability.

A fusion burn will result if the Z-pinch remains stable for a sufficiently long time, while the required high temperature and density are sustained. Ignition is possible if the fusion products are sufficiently well-confined. This will occur if the azimuthal magnetic field is sufficiently intense that fusion α-particles are confined, that is, $\rho_\alpha \ll R_{\rm pinch}$, where ρ_α is the α-particle gyro-radius and $R_{\rm pinch}$ is the compressed pinch radius. Following stagnation the pinch disintegrates rapidly, due to the rebound in plasma pressure and the accumulated effect of instabilities.

Z-pinches are susceptible to the Rayleigh–Taylor (RT) instability during implosion. Many techniques have been developed to control the effect of the RT instability, all directed toward maximizing the accumulated pinch energy. The most common techniques consist of altering the load configuration to provide a more uniform, initial mass distribution, or reducing the time needed to obtain a uniform, highly conducting plasma at current initiation. Other approaches involve decreasing the risetime of the current pulse and using concentric, multi-layer mass distributions.

The gas-puff Z-pinch was developed in the 1970s as a stable alternative to the more widely used wire-array Z-pinches (Shiloh et al. 1978) and it has demonstrated a surprisingly large range of scalability; it has been implemented on short and long implosion time generators, with risetimes $\tau_{1/4}$ ~0.1–1 μs and load currents $I_{\rm load} \sim 0.1$ to 10s of MA. Gas-puff pinches have also been configured to study gas mixtures. Gas-mixture Z-pinches have demonstrated a unique ability to produce a higher energy radiated spectrum and higher X-ray yield than a Z-pinch of either gas imploded separately (Bailey et al. 1986; Chang et al. 1991; DeGroot et al. 1997; Chaikovsky and Sorokin 1997; Levine et al. 2006; Qi et al. 2008). Multi-layer gas-puff implosions have also produced better results than single-layer or uniform-fill Z-pinches.

The improvements observed for gas mixtures and multi-shell implosions suggests that there is a complex interplay of shock-driven compressional heating, current diffusion, flux compression, and radiation transport at work, for which further analysis will provide deeper insights (Rostoker and Tahsiri 1978; Velikovich et al. 1996; Glazyrin et al. 1997; DeGroot et al. 1997). Staging the implosion, to optimize these dynamical processes, is expected to have specific benefits for fusion (Rahman et al. 1989, 1995, 2004; Ney et al. 2001). A gas-puff mixture of deuterium and argon was tested recently, with a reported neutron yield of Y ~3.7–3.9×10^{13} (Coverdale et al. 2007); modeling suggests that the neutrons are thermonuclear (Coverdale et al. 2007).

The configuration analyzed here is referred to as a 'Staged Z-pinch' and consists of a high-atomic-number plasma liner imploding onto a solid-fill hydrogenic target: for example, Xe onto deuterium–tritium (DT). We have studied this configuration for some time. This specific name was applied to characterize sequential, energy-transfer processes that occur in these more complex load configurations, leading to faster risetimes in the presence of improved stability.

As the current builds in the Staged Z-pinch and the outer liner begins to accelerate, shocks form, transporting current and energy radially inward toward

the target. As the shock collides with the DT, a secondary shock is produced in the target that also transports current and energy, pre-heating the target. As the liner continues to accelerate and compress the target, a fusion burn begins in the presence of a flux-compressed, ultra-high magnetic field. The ultra-high magnetic field confines fusion α-particles, providing an additional source of heat for the DT, raising its temperature to 50 keV and causing ignition in a magneto-inertial compression. For a precise set of initial-implosion parameters, net fusion energy is produced. In the absence of shocks the radial compression ratio needed for fusion to occur, by adiabatic compression alone, would be much higher. These are the findings reported here.

The discussion proceeds as follows: Sec. 2 discusses the growth of RT instability and its effect on energy coupling; Sec. 3 simulates the compression of a Staged Z-pinch, for different initial parameters; Sec. 4 describes the optimum configuration for fusion breakeven; and Sec. 5 concludes the paper.

2. Growth of the RT instability

A typical Z-pinch is RT unstable during implosion, since the implosion involves a light fluid (the magnetic field) accelerating a heavy fluid (the plasma). In the linear regime of analytic modeling, plasma perturbations grow as (Rahman et al. 2004)

$$\xi = \xi_0 e^{\gamma t} \tag{1}$$

where ξ_0 is the initial perturbation, $\gamma = \sqrt{gk}$ is the growth rate, g is the acceleration, k is the wavenumber, and t is the time. Approximating the distance, R, over which the Z-pinch plasma is accelerated as $R = gt^2/2$, (1) may be re-written as

$$\xi = \xi_0 e^{\sqrt{2Rk}} \tag{2}$$

and for a given mode number the perturbation growth depends exponentially on the distance over which the plasma is accelerated. Hence, Z-pinch implosions from a small initial radius are preferred.

The accumulated Z-pinch energy (in Gaussian units) can be estimated roughly as the work done on the pinch,

$$W = \int \mathbf{F} \cdot d\mathbf{r} = \frac{I^2 h}{c^2} \ln\left[R_\mathrm{i}/R_\mathrm{f}\right] \tag{3}$$

where I is the current, h is the axial length of the pinch, R_i is the initial radius, and R_f is the final radius of the pinch. Thus, high current and large radius implosions are preferred. The combined implications of (2) and (3) are that the radius must be chosen judiciously to avoid instability, while accumulating high energy in the pinch.

3. Simulations

The simulated Z-pinch load configuration is a 1.5 cm long, 0.2 cm thick Xe plasma liner imploding onto a DT target, as shown in Fig. 1. The initial Xe mass distribution is Gaussian and the DT target is uniformly-filled. The 'cold-start' initial plasma temperature is 2 eV, for both the Xe and DT.

The implosion dynamics are simulated with MACH2, which is a single-fluid, magneto-hydrodynamic, $2\frac{1}{2}$-dimensional, time-dependent code that treats the

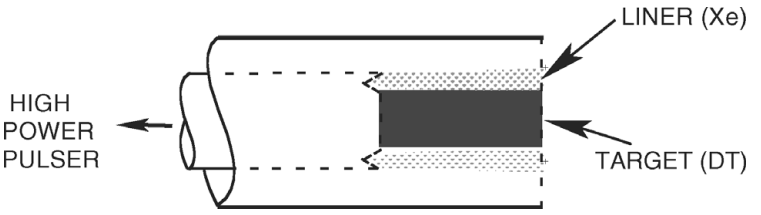

Figure 1. Schematic illustration of the Staged Z-pinch.

electron, ion, and radiation temperatures separately and calculates resistive and thermal diffusion using established transport models (Peterkin et al. 1998). The plasma equation-of-state is determined from SESAME look-up tables†. The Xe calculation uses the SESAME tables for thermal conductivity and electrical resistivity. A Spitzer model is used for the DT thermal conductivity and electrical resistivity, since this data is not readily available in the SESAME tables. MACH2 calculates flux-limited, single-group, implicit radiation diffusion. Ohm's law includes the Hall effect and thermal source terms for magnetic fields.

The plasma volume was resolved into 160 radial cells and 120 axial cells for 2D simulations, which was sufficient to model axial instability wavelengths as small as 0.3 mm. A random seed perturbation of 0.01 (1%) was applied throughout the simulation volume. This seed value is arbitrary, yet is typical for plasma liner simulations of this type. For comparison, a value of 25% is typically used for wire-array simulations.

The MACH2 code includes a self-consistent circuit model for the pulse power driver parameters (inductance, capacitance, and resistance) and the dynamically computed pinch-plasma parameters (inductance and resistance). For our simulation the assumed short-circuit discharge parameters, resistance, inductance, capacitance, and charging voltage were $R = 0$, $L = 10$ nH and $C = 0.35$ μF, and $V_0 = 3.4$ MV. The capacitor-stored energy is $1/2\ CV_0^2 = 2$ MJ and the current pulse risetime is $\tau_{1/4} \simeq 95$ ns. The discharge electrodes are assumed to be perfectly conducting.

MACH2 was run first in a 1D mode, for a fixed pinch implosion time of 121 ns, to determine the load masses, M, needed to implode from the following initial radii: $R_\mathrm{i} = 2.0$, 1.5, 1.0, and 0.5 cm. For zero-dimensional modeling this is equivalent to keeping $MR_\mathrm{i}^2 =$ constant for a given current profile. These 1D mass parameters were then used as inputs for the 2D simulations. The respective mass densities for Xe (in order of decreasing radius, 2.0–0.5 cm) were $\rho_\mathrm{Xe} = 1.3 \times 10^{-3}$, 4.2×10^{-3}, 1.7×10^{-2}, and 0.18 g cm^{-3}. The respective mass densities for DT were $\rho_\mathrm{DT} = 9.4 \times 10^{-5}$, 5.5×10^{-5}, 47.8×10^{-5}, and 3.4×10^{-3} g cm^{-3}. Note that the total mass of the DT is several orders of magnitude smaller than that for the Xe.

Figure 2 plots the load-current time profile, I_load, for the 0.5 cm radius case. A peak current of $I_\mathrm{load} = 17$ MA is obtained in 80 ns. After the peak the slope of the I_load waveform changes dramatically, due to the large increase in inductance caused by the decreasing radius of the pinch, since $L_\mathrm{pinch}(t) = \mu_0/2\pi \ln[R_\mathrm{out}/R_\mathrm{pinch}(t)]$, where R_out is the radius of the return-current boundary path and $R_\mathrm{pinch}(t)$ is the time-dependent pinch radius. Maximum compression of the Z-pinch occurs at 121.17 ns, when the discharge current is approximately $I_\mathrm{load} \simeq 8$ MA. After this time

† http://t1web.lanl.gov/doc/SESAME_3Ddatabase_1992.html

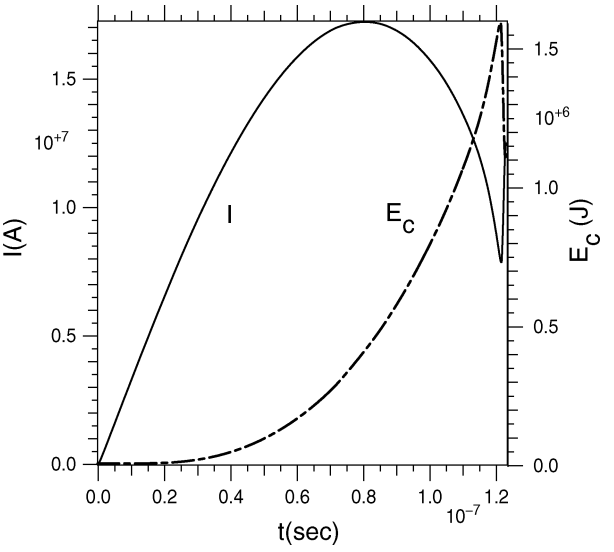

Figure 2. Load current, I, and the extracted circuit energy, E_c, for the 0.5 cm radius pinch.

the pinch radius expands and the discharge current rebounds. This time-dependent behavior of the current pulse is typical for all pinch radii that were simulated.

The time profile for the total energy extracted from the circuit, E_c, is also displayed in Fig. 2, where $E_c = E_{\text{radiation}} + E_{\text{transport}} + E_{\text{kinetic}} + E_{\text{thermal}} + E_{\text{inductive}}$, that is the sum of the energy lost by dissipation (through radiation and transport), pinch energy (kinetic and thermal), and system energy (inductive magnetic). As illustrated, E_c continues to increase until the moment of peak compression, reaching a peak value of $E_c = 1.6$ MJ. The balance of the initial stored energy at this time remains in the circuit capacitance and is equal to 0.4 MJ. After peak compression E_c decreases rapidly, indicating, as discussed below, that energy is added back into the circuit as the pinch explodes due to the onset of fusion.

Figure 3 compares graphically the level of instability computed at 100 ns, as a function of the initial pinch radius. Shown are 2D plots of the pinch current density. In these illustrations the R axis is horizontal and the Z axis is vertical and the scale units are centimeters. In qualitative agreement with (2), the level of instability is greatest for the largest initial radius and smallest for the smallest initial radius.

For the 2.0 cm initial radius simulation the calculation terminates at 101 ns, as the pinch becomes unstable and the discharge current path is broken. The result is similar for the 1.5 cm initial radius simulation, which terminates at 102 ns. For both the simulated neutron yield was insignificant.

For the 1.0 cm radius simulation Fig. 3 shows that the liner's outer surface is slightly unstable. At the inner radius edge of the liner is a stable detached current layer, illustrating how a multi-liner cascade can improve stability. The 1.0 cm simulation terminated at 115 ns, due to instability and the neutron yield was $Y = 2.7 \times 10^{13}$.

The 0.5 cm radius implosion provides the best stability, as shown in Fig. 3. At this time both the liner and target surfaces remain stable. The detached current layer, evident in the preceding panel, has broadened for this radius and is located

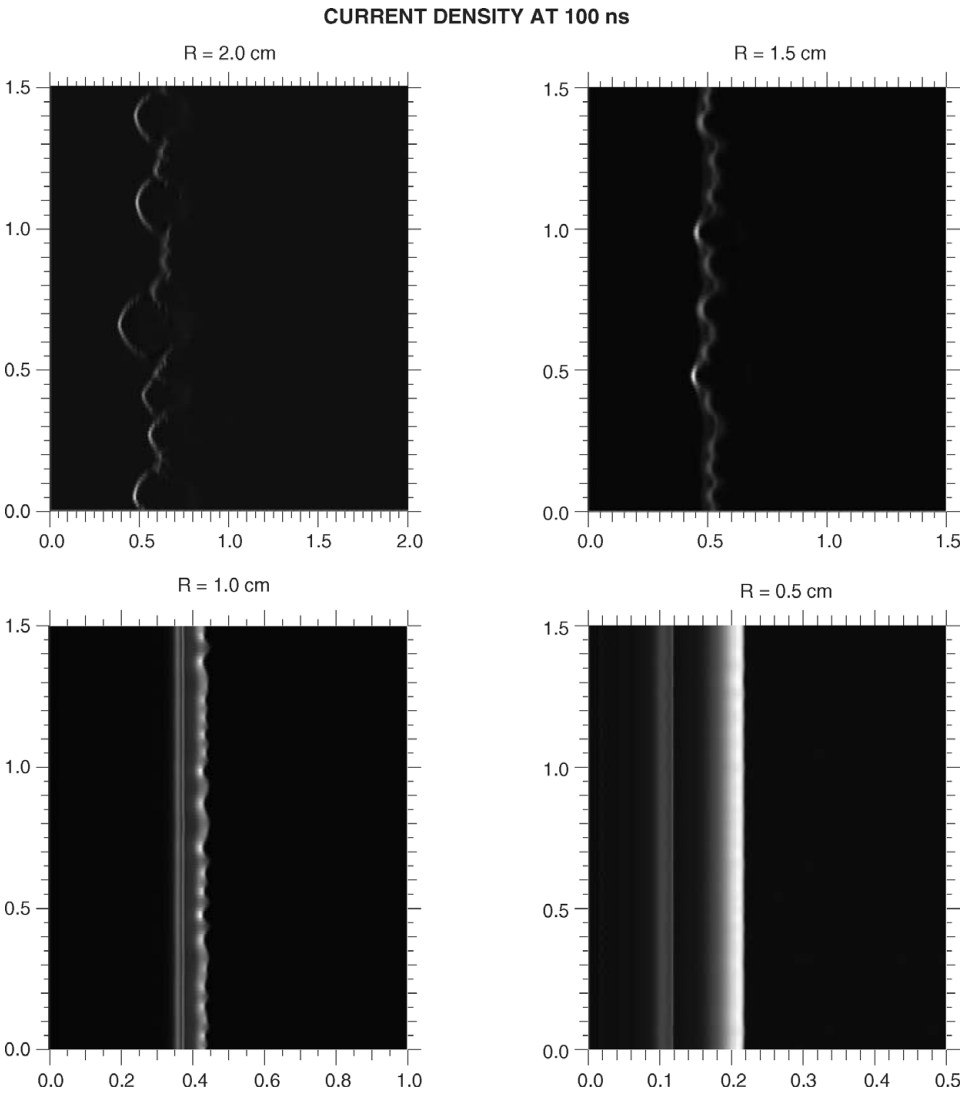

Figure 3. Current density (R–Z) iso-contour profiles computed 100 ns into the implosion as a function of the initial radius: $R_i = 2.0$ cm, 1.5 cm, 1.0 cm and 0.5 cm. The horizontal and vertical axes correspond to the radial and axial coordinates, respectively, and the units are in centimeters. White color corresponds to highest-computed intensity.

at the outer surface of the DT target. The 0.5 cm radius case is now examined in more detail.

4. Detailed discussion for the 0.5 cm radius implosion

Figure 4 displays a time sequence of 2D (iso-contour) discharge current density images for the 0.5 cm radius implosion, beginning at 80 ns and progressing to 123 ns, just after peak compression of the pinch, which occurs at 121.17 ns. Note the radial scales in subsequent images: it is largest for the 80 ns panel and shortest for the last three panels (121.17, 122, and 122.5 ns). These images extend in time those that

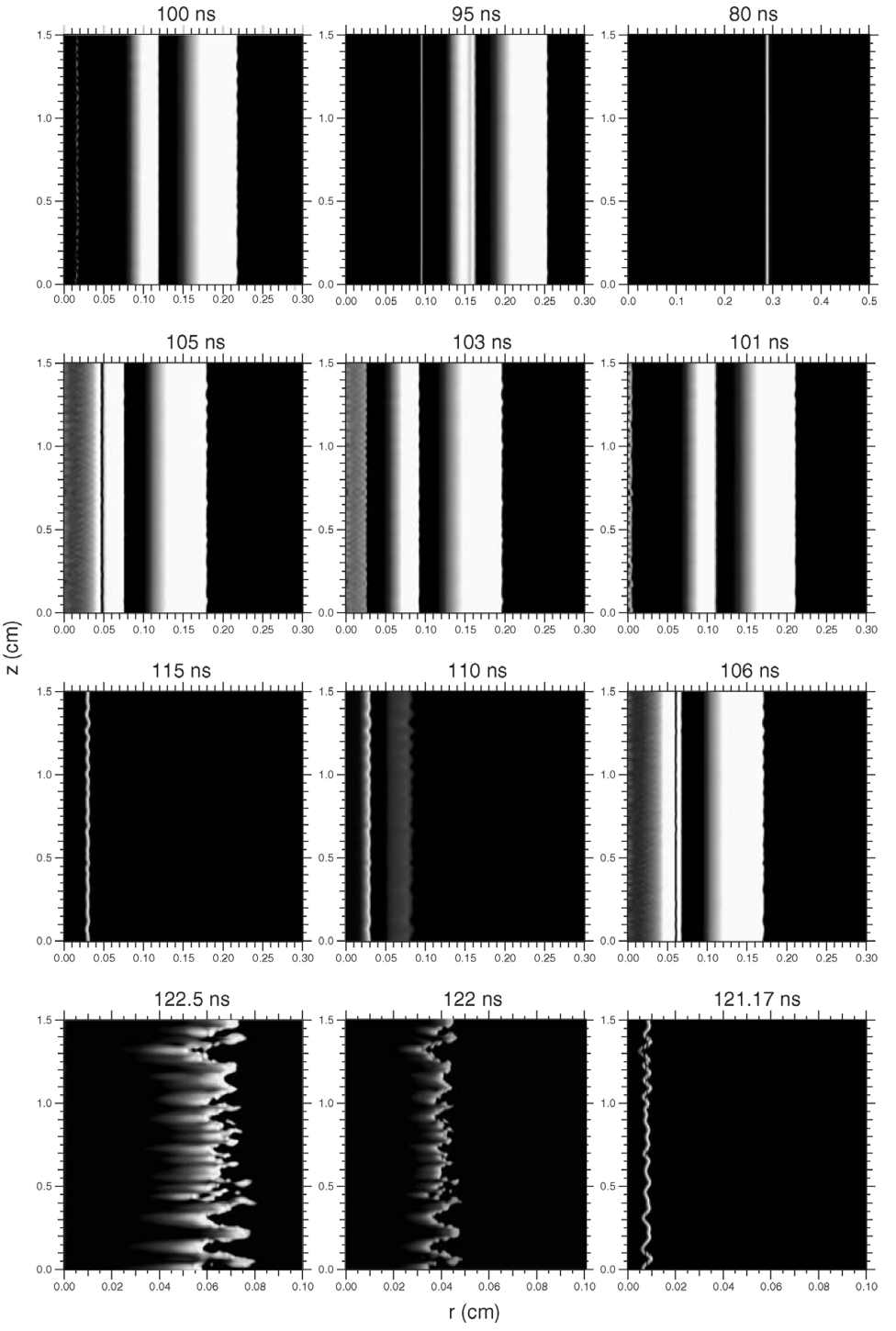

Figure 4. *R–Z* profiles of axial current density for a 0.5 cm initial radius.

are shown in Fig. 3, illustrating the stability of the 0.5 cm radius implosion up to peak compression, when the RT instability develops rapidly and within a couple of nanoseconds the pinch disassembles. The RT instability at the DT surface is due to deceleration of the liner against the internal pressure of the target plasma and then subsequent expansion outward as the target plasma explodes.

An axial average of the data in Fig. 4 is also displayed as line plots in Fig. 5. At 80 ns the outer radius of the pinch is at 0.34 cm, having imploded from its initial value of 0.5 cm. At this time the current density is concentrated in a narrow sheath between 0.28 cm and 0.29 cm inside the DT and a more diffuse layer distributed between 0.3 cm and 0.34 cm radius inside the Xe. Until peak compression the value of the current density at the outer surface of the Xe remains at a nominal value of $J_z = 3\text{–}5 \times 10^{12}$ A m^{-2} accelerating the outer surface of the Xe by the $\mathbf{J}_z \times \mathbf{B}_\theta$ force.

As time progresses, the current density is transported into the DT interior by shocks, which are labeled in the illustrations. Shocks develop when the liner temperature remains low and the density high (DeGroot et al. 1997). The specific choice of Xe, as a high-Z liner material, enhances the generation of shocks, by radiative cooling.

At 95 ns, when the outer radius of the pinch has decreased to 0.25 cm, there are three layers of high current density: an outer layer between 0.2 cm and 0.25 cm radius, a thinner layer between 0.12 cm and 0.15 cm, and a third layer at 0.09 cm. The Xe shock is characterized by a spike in J_z that is located at the Xe–DT interface and a more diffuse region extending into the DT. A second shock is present inside the DT that is generated when the Xe shock collides with the outer surface of the DT.

As time increases the DT shock converges to the axis and reflects. The outwardly propagating current layer splits into layers of positive and negative current density. As the shocked layer expands outward, a self-consistent current loop is established inside the pinch that supports flux compression. The amplitude of the negative current density layer continues to grow as the liner implodes.

At 121.17 ns the positive and negative current densities have approximately equal values at 2.6×10^{15} A m^{-2}. The radius of the inner layer is 0.006 cm and the radius of the outer layer is 0.011 cm. Until this time the magnitude and thickness of the current density at the outer surface of the Xe liner remains relatively constant, but beyond this point it begins to diminish and the implosion continues to be driven largely by liner inertia.

Throughout the implosion there is a complicated evolution and interplay of the current density layers and their magnitudes. Even though the current densities are comparable in magnitude until peak compression, the current layer thicknesses are unequal. Integrating J_z as a function of radius confirms the presence of the current loop. Near peak compression the magnitude of this loop current is $I_{\text{loop}} \simeq 25\text{–}30$ MA, while the total circuit current remains as indicated in Fig. 2. The inductance of this current loop is approximately 0.7 nH, with an equivalent inductive energy of 0.2–0.3 MJ.

Examination of the corresponding azimuthal magnetic field, B_θ, facilitates further insight. At 115 ns, in Fig. 6, B_θ attains a peak value of about 27 MG at the outer surface of the liner, whereas at the surface of the DT B_θ has a peak value of 44 MG. It is this larger magnetic field, located at the target surface, that is due to flux compression, driven by the inertial pressure of the liner (Rahman et al. 1995).

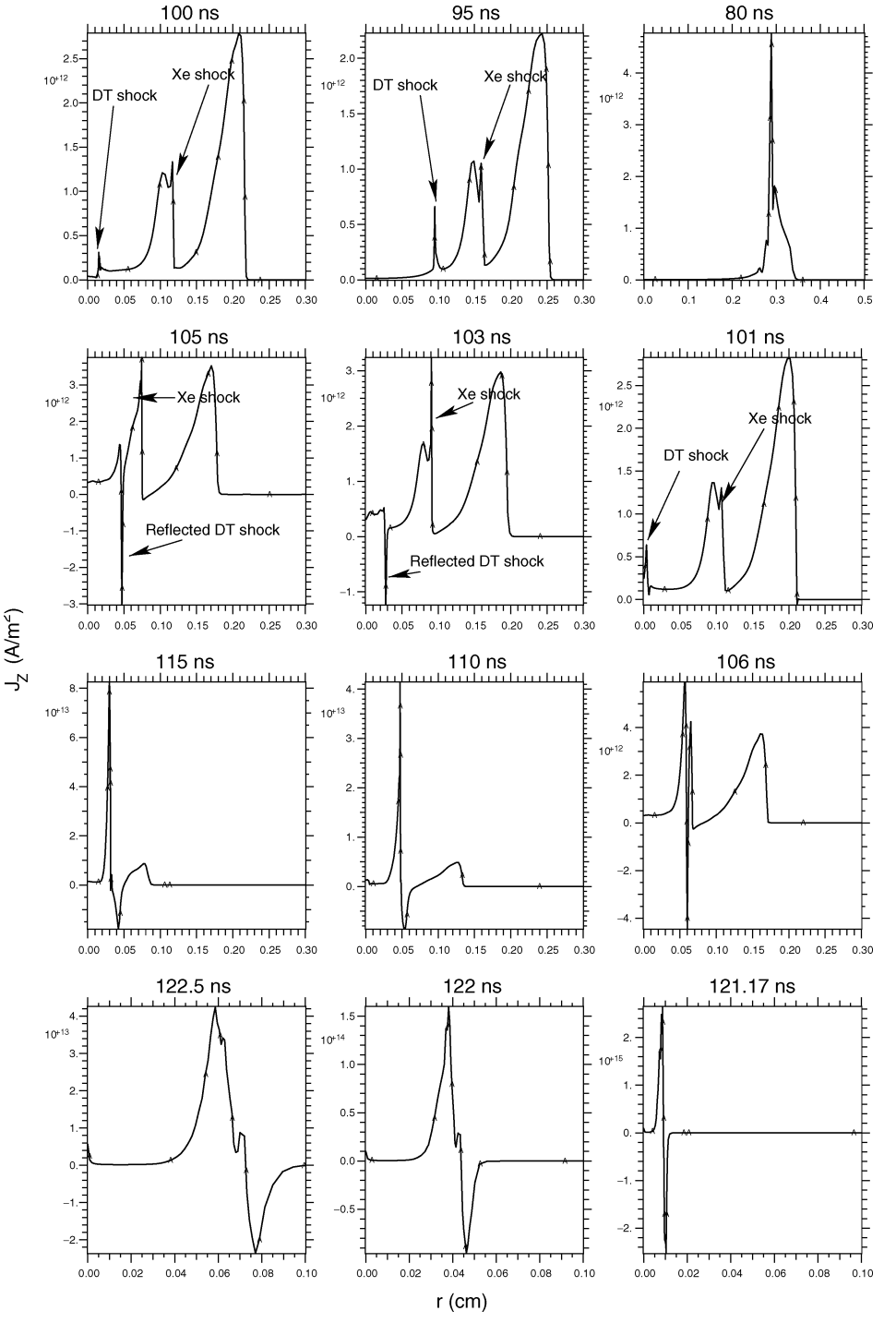

Figure 5. Axial current density averaged over the axial direction.

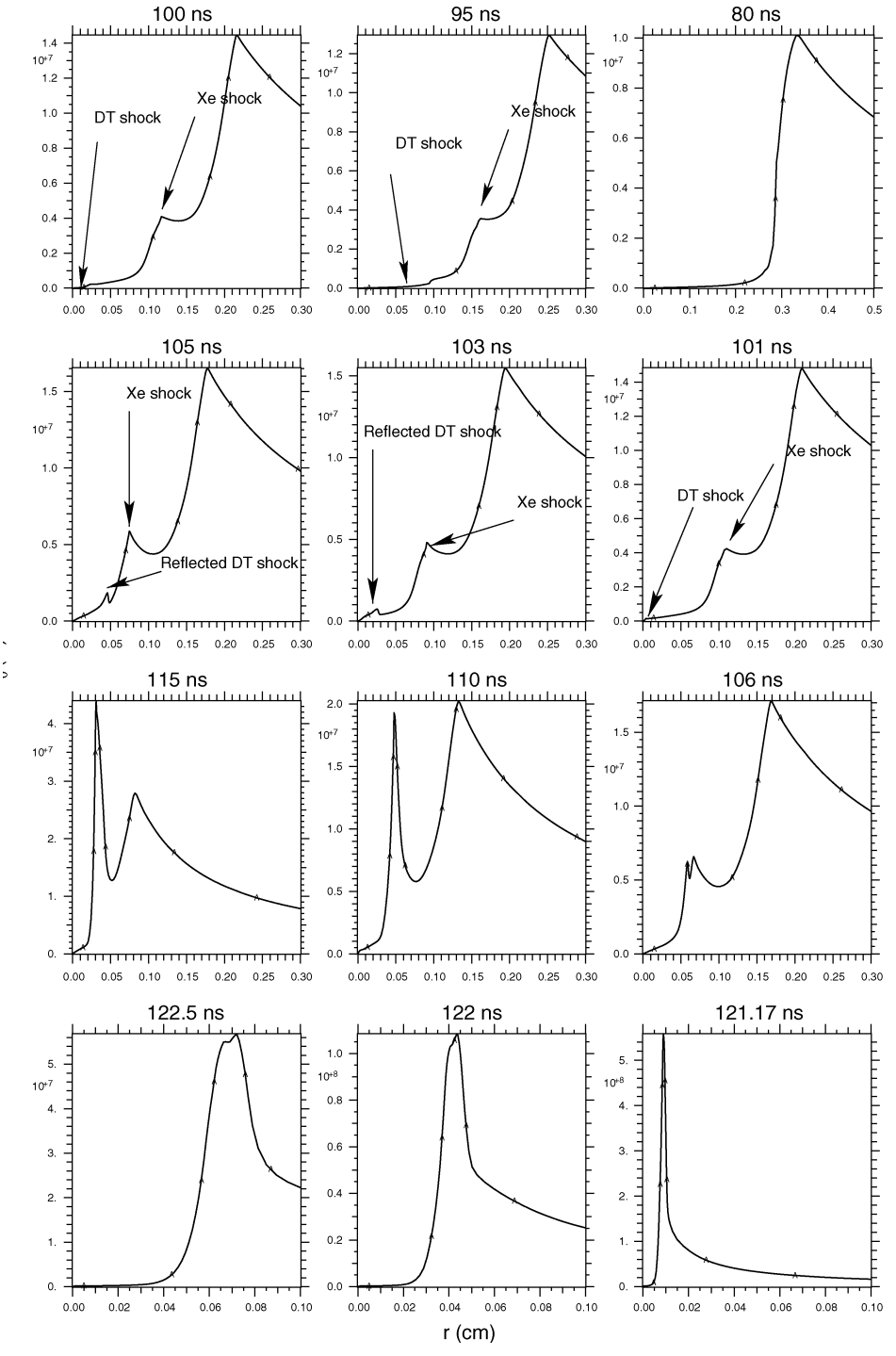

Figure 6. Azimuthal magnetic field averaged over the axial direction.

At 121.17 ns B_θ attains a peak value of 560 MG. At 122 ns the value of B_θ has decreased to 100 MG as the pinch re-expands.

The ion density, N_i, and temperature, T_i, panels are displayed in Figs 7 and 8, respectively. The electron and ion temperatures remain in thermal equilibrium, until the moment of peak compression, when the fusion α-particles heat the ions more rapidly than the electrons.

The 80 ns panels show a sharp transition in density and temperature near the 0.3 cm radius, with $n_\mathrm{i} \simeq 6{\times}10^{21}$ cm^{-3} and $T_\mathrm{i} \simeq 115$ eV. Notice that the peak density and temperature do not coincide, as the higher temperature peak and lower density corresponds to the shocked DT, whereas the higher density peak and lower temperature corresponds to the radiatively cooled Xe. As time increases, shocks continue to propagate in the DT. The shocks then reflect off the axis causing the density and temperature values to oscillate. By 115 ns the nominal density and temperature of the DT has reached $n_\mathrm{i} = 8 \times 10^{22}$ cm^{-3}, and $T_\mathrm{i} = 400$ eV. At peak compression, 121.17 ns, the peak ion density in the DT is $n_\mathrm{i} = 10^{24}$ cm^{-3}, and the temperature is $T_\mathrm{i} = 54$ keV, whereas the peak ion density in the Xe is three times higher at $n_\mathrm{i} = 3{\times}10^{24}$ cm^{-3}, and the temperature is much lower. The large increase in temperature at this time is attributed to ion heating by the fusion α-particles, as will be discussed shortly.

These density and temperature values in the DT are sufficient for fusion to occur. Based on the Lawson criterion, $n\tau > 10^{14}$ cm^{-3} s, a confinement time of $\tau = 30$ ps is needed, which is well satisfied.

Shocks play a key role in the Staged Z-pinch, pre-compressing the target plasma prior to the onset of fusion. In the present case the DT is compressed from a 0.3 cm radius to a final radius of 0.005 cm, which is a factor of 60, cf. Figs 7 and 8, producing a temperature increase from 2 eV to 60 keV.

To achieve the same temperature increase in the DT without shock heating, that is by adiabatic compression alone, the radial compression ratio of the DT would need to be much higher. For adiabatic compression the initial and final plasma temperatures are related to the initial and final radii by $T_\mathrm{f} = T_\mathrm{i}(R_\mathrm{i}/R_\mathrm{f})^{2(\gamma-1)}$, where $\gamma = 5/3$ is the ratio of specific heats for DT. Hence, to achieve the same temperature increase noted above, the compression ratio would need to be $R_\mathrm{i}/R_\mathrm{f} \simeq 2.5 \times 10^3$. Thus, shock heating is a important component in preparing the DT target for fusion conditions.

Consider the Mach number $M = V_\mathrm{r}/C_\mathrm{s}$, where V_r is the radial implosion velocity and $C_\mathrm{s}^2 = \partial P/\partial\rho$ is the sound speed, P is the pressure, and ρ is the density. The Mach number was calculated at each simulation grid point based on this equation; the results are displayed in Fig. 9.

At 80 ns a Mach 2.2 shock is present at a 0.27 cm radius, just inside the DT. At 95 ns, when $V_\mathrm{r} = 4$ cm μs^{-1}, two shocks are clearly evident: one located at the Xe–DT interface and another located inside the DT, at a 0.093 cm radius, confirming the labels shown in preceding figures. The lower Mach number for DT is due to the high sound speed in DT. During the next few nanoseconds the DT shock diminishes in amplitude, as it converges to the pinch axis, reflects, and then recollides with the imploding Xe shock at 106 ns.

At peak compression the DT ignites, and a radially expanding shock is generated on the axis. At this time the pinch outer radius is $R_\mathrm{f} = 0.01$ cm and the azimuthal magnetic field is $B_\theta = 560$ MG. Such a high-intensity magnetic field traps the fusion α-particles inside the target, providing an additional source of heating for target

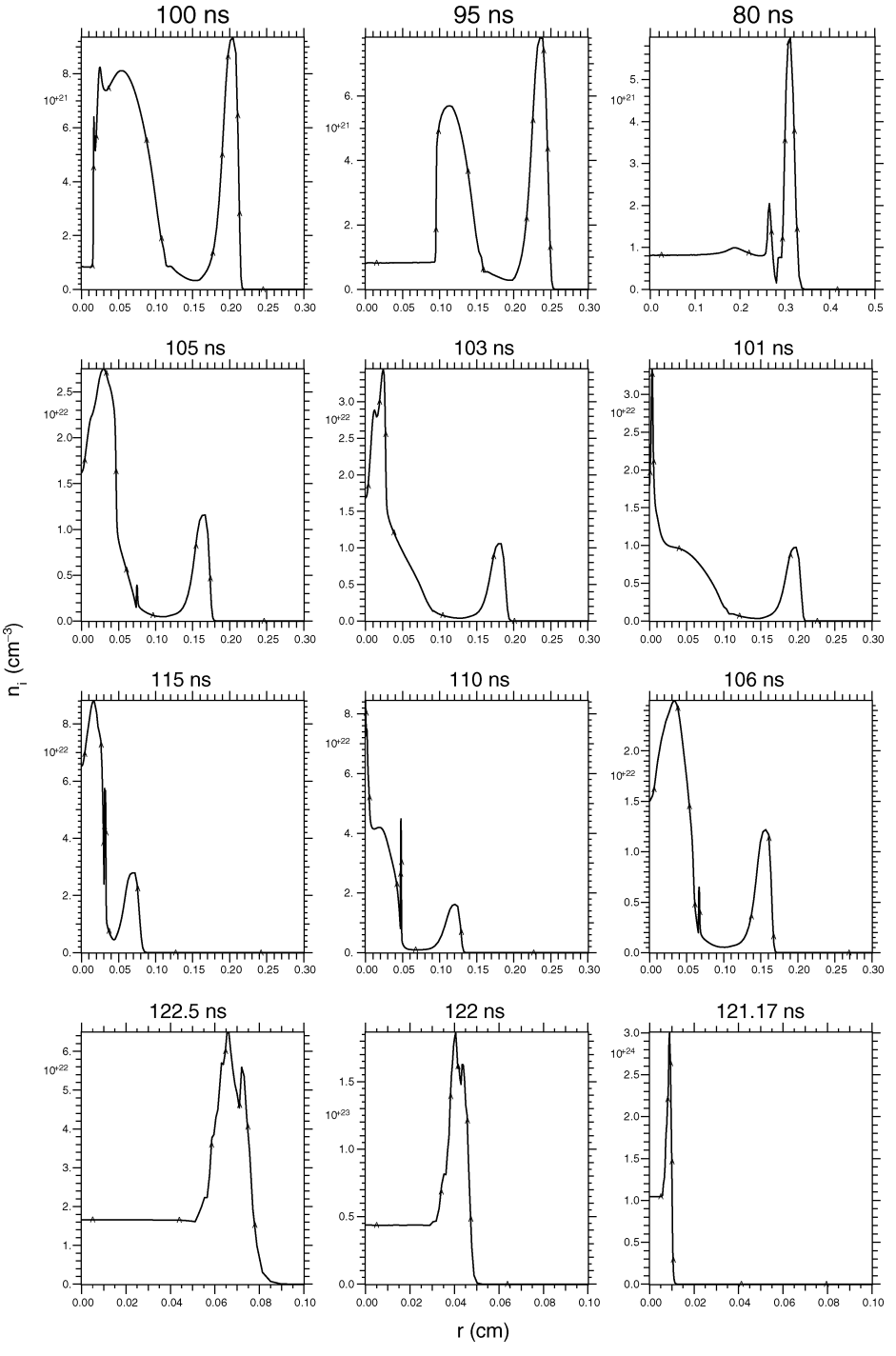

Figure 7. Ion density averaged over the axial direction.

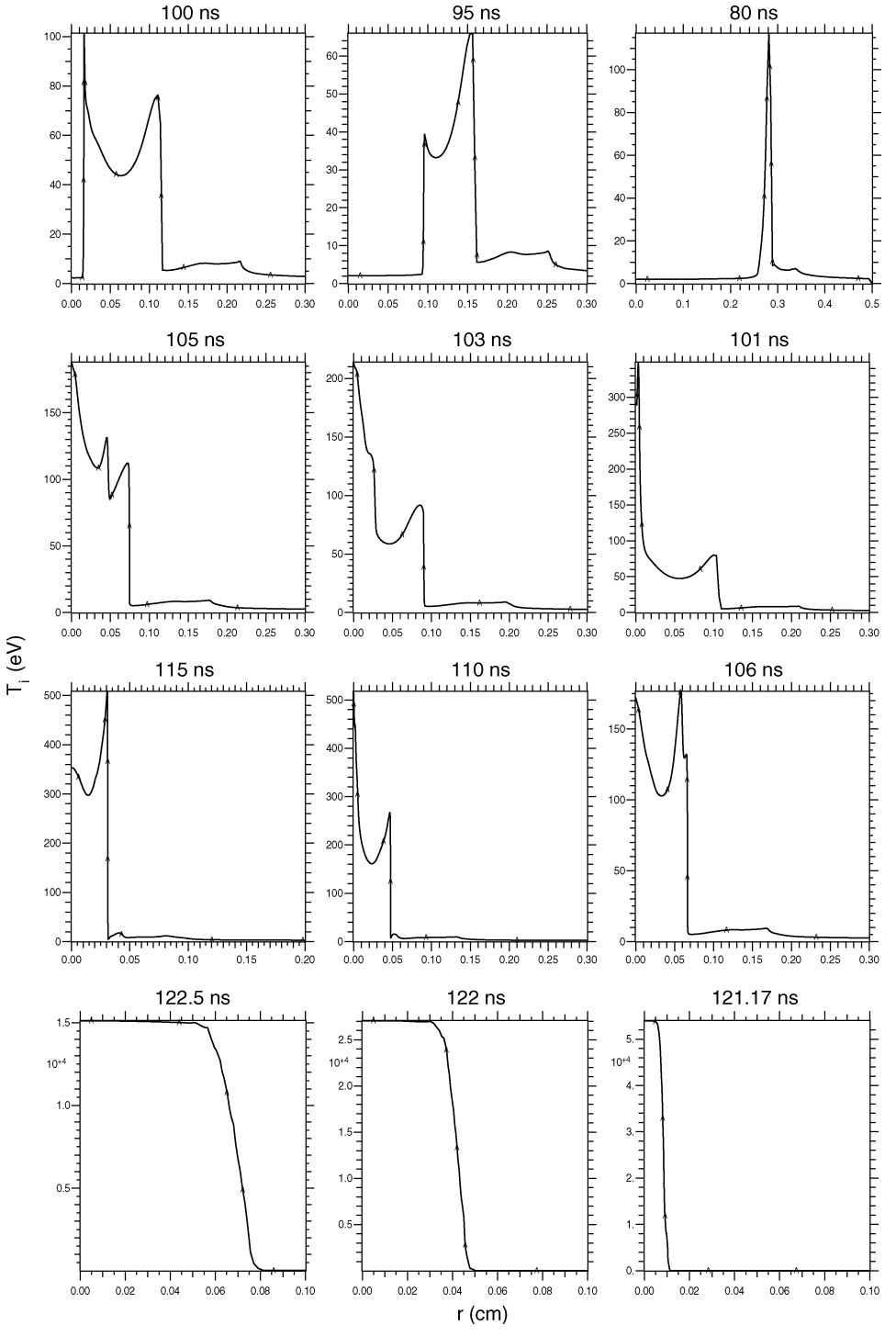

Figure 8. Ion temperature averaged over the axial direction.

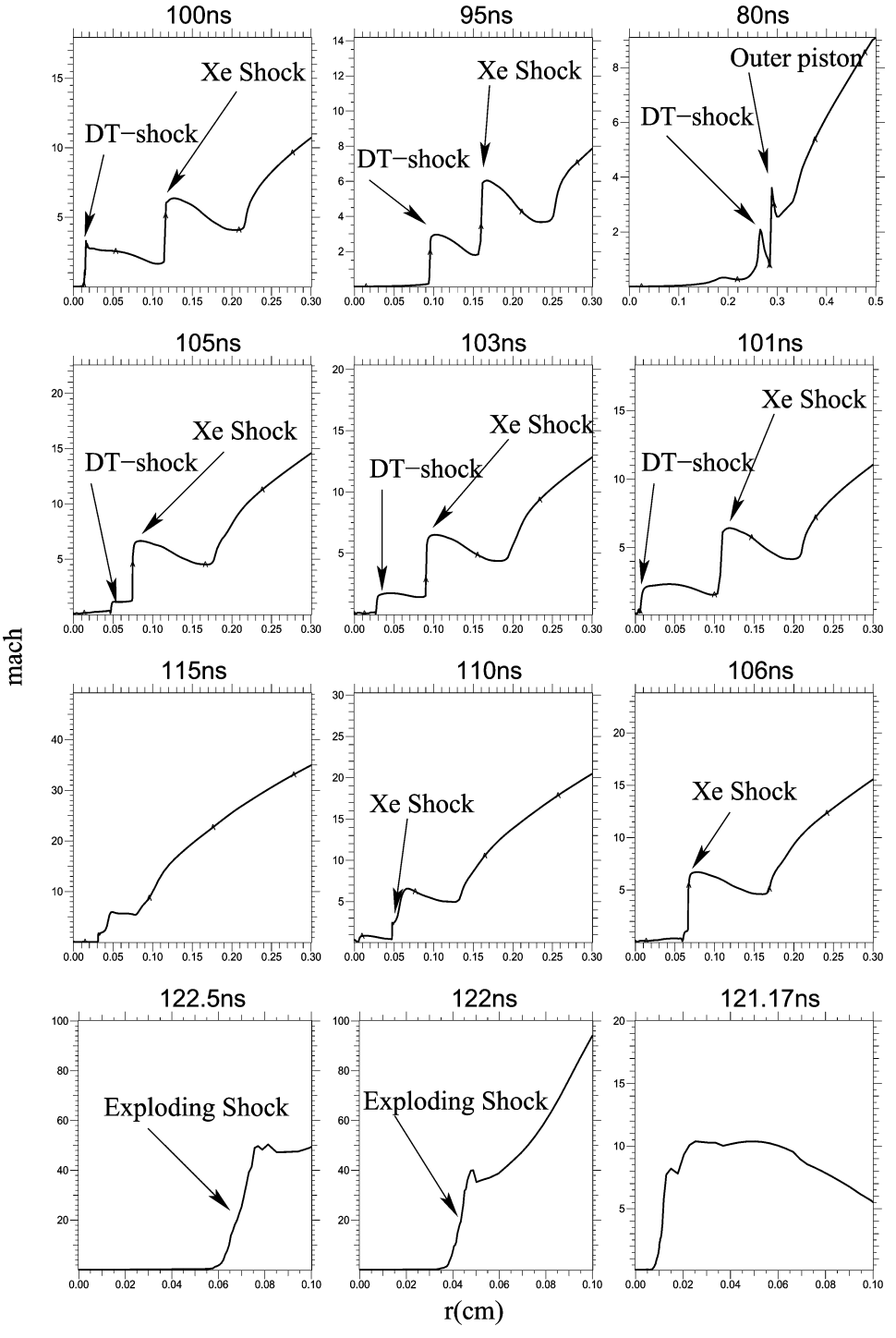

Figure 9. 'Line-outs' of mach number averaged over the axial direction.

ignition. When the DT plasma pressure exceeds the inertial pressure of the liner, the pinch explodes, driven by the production of internal energy.

Some flux leakage occurs, but we assume that most of it remains during the fusion burn. Assuming an average value for B_θ of 100 MG and a 3.5 MeV α-particle energy, the corresponding α-particle gyroradius would be $\rho_\alpha = 0.002$ cm, which is roughly an order of magnitude less than the final pinch radius, R_f.

Based on the 1D line averages presented above, nearly all of the initial Xe mass participates in the implosion and is compressed into a thin layer, approximately 0.001 cm thick, at the outer surface of the DT, at peak implosion, with an average radius of 0.01 cm. Although some instability is evident at this time, with an approximate wavelength of $\lambda = 1$ mm, the effect of instability is exaggerated by the expanded radial scale displayed here, relative to the axial scale length. For the most part the pinch remains largely intact and stable as the fusion burn proceeds.

Figure 10 provides a summary of the simulated pinch parameters at 121.17 ns (ion density, ion temperature, axial current density, and magnetic field). Also indicated are the peak values for each parameter, e.g., $\hat{n}_\mathrm{i}, \hat{J}_z, \hat{T}_\mathrm{i}, \hat{B}_\theta$, obtained from the 1D line outs above. Note the magnified radial scale of these images, relative to previous figures.

The illustrations in Fig. 10 provide a good indication of the final radial compression ratio for the pinch at peak implosion. Taking an initial radius of $R_\mathrm{i} = 0.5$ cm and a final radius of $R_\mathrm{f} = 0.0067$–0.011 cm, the pinch compression ratio is in the range $R_\mathrm{i}/R_\mathrm{f} \simeq 45$–$75$. Radial compression ratios of 40–45 have been reported in an experimental configuration similar to the one analyzed here, that is for a multi-shell, gas-puff implosion (Failor et al. 2007; Chaikovsky and Sorokin 1997). At the higher end, a radial compression ratio in excess of 120 has been reported for an extruded-shell Z-pinch (Appartaim and Dangor 1998). So the compression ratio reported here is reasonable.

As shown in Fig. 4, less than a nanosecond after peak compression, the entire Z-pinch column becomes RT unstable and the pinch disintegrates (light-fluid DT plasma pushing against the heavy-fluid Xe liner). The last recorded output for data is at 122.5 ns, and the calculation stops at 123 ns.

The time evolution of the Staged Z-pinch energies are shown in Fig. 11 for the expanded time interval of $t = 118$–123 ns, including α-particle energy, E_α, implosion kinetic energy, E_k, ion energy, E_i, scaled neutron energy, $E_\mathrm{n} \times 0.248$, and scaled fusion energy, $E_\mathrm{f} \times 0.199$.

Near peak compression E_k decreases to zero, from a peak value of $E_\mathrm{k} = 0.6$ MJ at 118 ns as implosion kinetic energy is converted into plasma thermal energy. The ion energy begins to increase around 119 ns. At 120.9 ns E_i begins to increase rapidly to a peak value of $E_\mathrm{i} = 6$ MJ at 121.3 ns. The rapid increase in E_i at 120.9 ns is driven by compressional and α-particle heating. The pinch stagnation time is roughly given by the time interval between when E_i increases rapidly and E_k remains low. From Fig. 11 $t_\mathrm{stagnation} \simeq 0.3$ ns. Near the end of the fusion burn, at 121.2 ns, E_k begins to increase rapidly, as the Z-pinch internal pressure increases, rising to a peak value of 15.8 MJ at the end of the calculation.

The total fusion energy is equal to the sum of the neutron and α-particle energies, $E_\mathrm{f} = E_\alpha + E_n$, which attain their peak values at the end of the calculation, $E_\mathrm{f} =$ 84 MJ, $E_\alpha = 17$ MJ, and $E_\mathrm{n} = 67$ MJ and a neutron yield of $Y \simeq 3.0 \times 10^{19}$. This level of fusion energy is 42 times greater than the energy initially stored the circuit

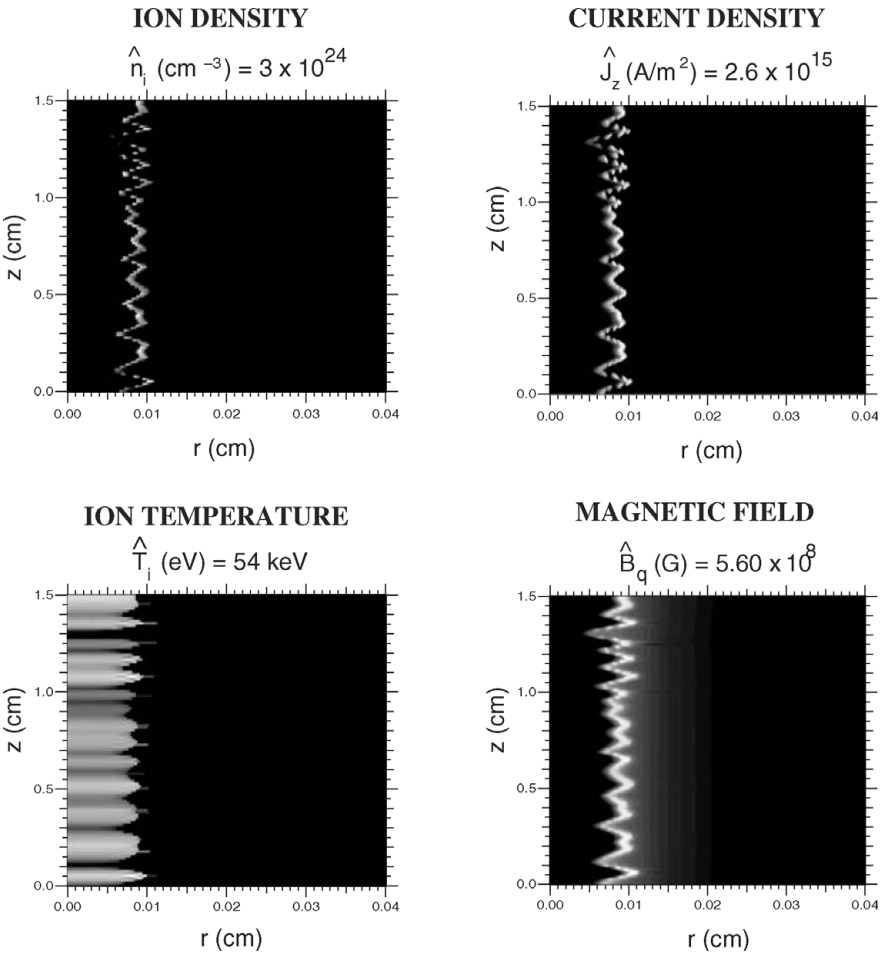

Figure 10. R–Z iso-contour profiles of (left to right, top to bottom) ion density, axial current density, ion temperature, and azimuthal magnetic field computed 121.17 ns into the compression. The peak parameter values are shown at the top each panel, as $\hat{n}_\mathrm{i}, \hat{J}_z, \hat{T}_\mathrm{i}, \hat{B}_\theta$.

capacitor. For comparison, our 1D simulations for the same configuration predict a 70 MJ yield.

Figure 12 shows the total ion heating power $P_\mathrm{i} = dE_\mathrm{i}/dt$ versus time, on a logarithmic scale. The full simulation time is shown in the inset. Four distinct time phases are evident, characterizing the implosion dynamics of the Staged Z-pinch. These phases are defined as the times when various ion-heating mechanisms dominate and are labeled as Ohmic, Shock, Adiabatic, and α-particle.

The value of P_i at early times in the inset is due to Ohmic heating, which dominates in the early phase of the implosion from 0–78 ns. This is the phase when the $\mathbf{J}_z \times \mathbf{B}_\theta$ force remains small and the Z-pinch plasma remains nearly at rest. As shown, there is a competition between the plasma pressure outward and the magnetic pressure inward, leading to a quasi-static equilibrium, where P_i oscillates (Felber 1982).

The shock heating phase begins at approximately 80 ns, as correlated with the density and temperature spikes shown in Figs 7 and 8. During this phase a shock

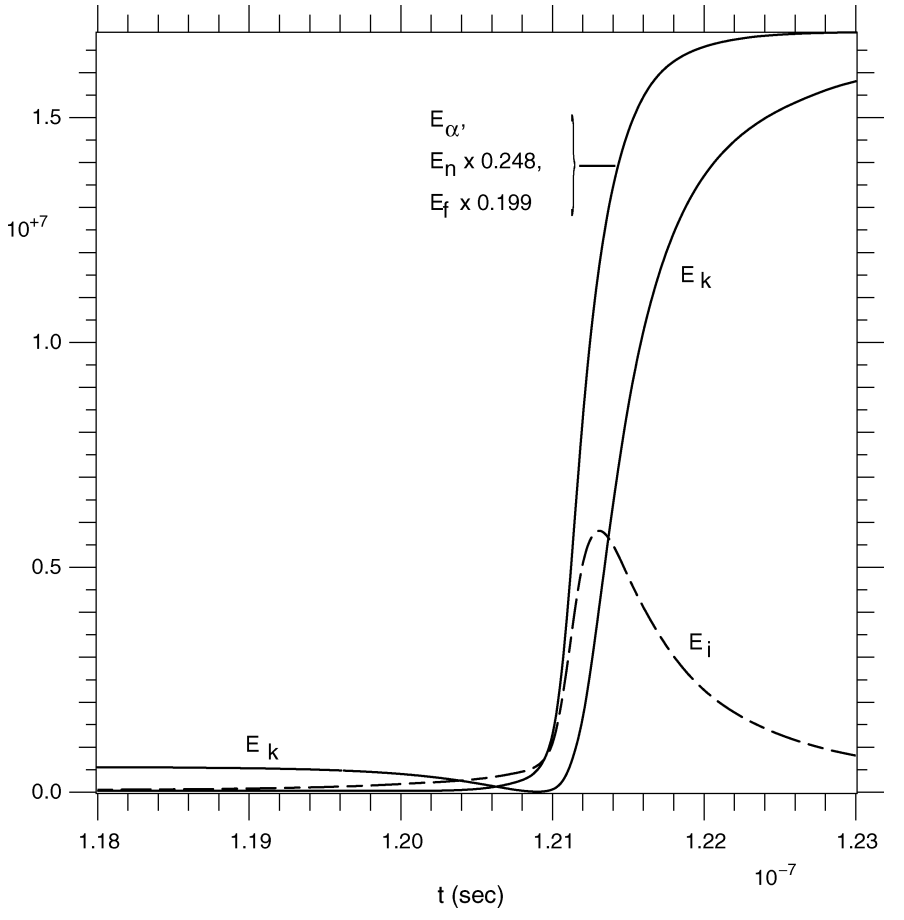

Figure 11. α-particle energy, E_α, liner kinetic energy, E_k, ion thermal energy, E_i, scaled neutron energy, $E_\mathrm{n} \times 0.248$, and scaled total fusion energy, $E_\mathrm{f} \times 0.199$, plotted as functions of time.

propagates toward and reflects off the pinch axis, rapidly heating the target at a one to two orders of magnitude higher power level than during the Ohmic phase. The oscillation observed during the Ohmic phase, being several orders of magnitude less, is not observed during this and subsequent phases.

At 101 ns, the shock reflects off the axis and the target plasma temperature is about 150 eV. From 101 ns to 121 ns, shocks continue to reflect back and forth inside the target plasma contributing further to ion heating.

From approximately 115 ns onward, adiabatic heating dominates until approximately 120 ns. The onset of α-particle heating occurs during the final nanosecond, or so, when the target temperature increases rapidly to approximately 50 keV and the plasma releases the maximum amount of fusion energy.

5. Conclusions

This paper presents 2D simulations of a Z-pinch. The load is a 0.2 cm thick shell of Xe imploding onto a DT target (Staged Z-pinch). The system is driven by a 95 ns

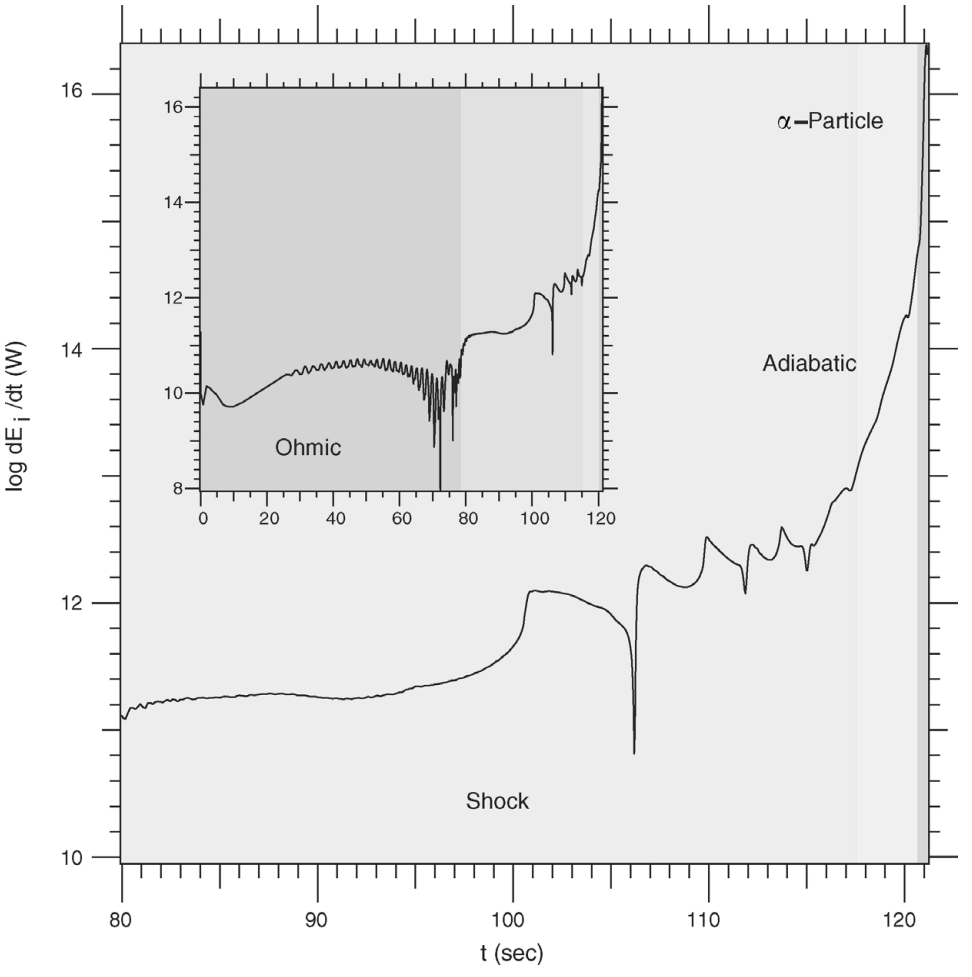

Figure 12. Log total ion heating power, $P_i = dE_i/dt$, plotted as a function of time. The inset shows the full simulation time from 0–123 ns.

risetime, 17 MA, 2 MJ pulser. The 2D simulations were performed using MACH2, a sophisticated radiation-hydrodynamics code.

We have considered several cases for the pinch initial radius, ranging from 2.0 cm down to 0.5 cm. The implosion dynamics are very sensitive to the choice of the initial radius, the atomic composition of the liner mass, and the final pinch stability.

High performance is obtained through careful optimization of these parameters, i.e. the liner thickness, the liner mass distribution, and the target mass. The best stability is produced for the smallest initial radius simulated. The pinch produces precisely timed shocks that originate in the Xe liner and are transmitted across the mass boundary, into the DT target. Target shocks reflect inside the DT as it is compressed by the Xe liner. For the duration of the implosion the pinch remains stable. There exists a theoretical basis to account for enhanced stability in a shock-compressed implosion system (Rostoker and Tahsiri 1978; DeGroot et al. 1997).

The dwell time of the pinch at maximum compression is around 0.3 ns, as the pinch is compressed by the liner inertia, in the presence of an intense azimuthal

magnetic field; the latter is a result of flux compression. The implosion is accurately characterized as 'magneto-inertial' and produces a nominal radial compression ratio for the liner of 50 and a fusion energy gain that is 42 times greater than the stored, capacitor bank energy.

3D simulations of Z-pinches have appeared recently, directed principally toward the analysis of wire-array implosions (Chittenden et al. 2007; Yu et al. 2008). For wire-array loads a 3D simulation is critical, since the discrete nature of the wire-array load inevitably introduces azimuthal non-uniformities. However, for the small initial radius of a Staged Z-pinch, and for a uniform, solid-fill liner, a 3D simulation is not expected to be as critical. Indeed, even for our 1D calculations the predicted fusion energy yield was 70 MJ, which is less than 2D predictions for 85 MJ, where one would expect a lower yield because of the higher dimensionality. The higher yield for the 2-D simulation is probably due to the appearance of hot spots, generated at the first collapse of the on-axis shock.

Acknowledgements

This project was supported by the US Department of Energy. We acknowledge R. E. Peterkin and J. H. Degnan for their assistance in providing access to the MACH2 code.

References

Appartaim, R. K. and Dangor, A. E. 1998 Large magnetic fields generated by z-pinch flux compression. *J. Appl. Phys.* **84**(8), 4170–4175.

Bailey, J., Fisher, A. and Rostoker, N. 1986 Coupling of radiation and hydrodynamics in a z pinch plasma. *J. Appl. Phys.* **60**, 1939.

Chaikovsky, S. A. and Sorokin, S. A. 1997 Density, temperature, and size of a plasma produced in a single and double shell liner implosion. *The Fourth International Conference on High Density Z-Pinches*, Vol. 409. New York: American Institute of Physics.

Chang, T. F., Fisher, A. and Van Drie, A. 1991 X-ray results from a modified nozzle and double gas puff z pinch. *J. Appl. Phys.* **69**, 3447.

Chittenden, J. P., Ciardi, A., Jennings, C. A., Lebedev, S. V., Hammer, D. A., Pikuz, S. A. and Shelkovenko, T. A. 2007 Structural evolution and formation of high-pressure plasmas in x pinches. *Phys. Rev. Lett.* **98**(2).

Coverdale, C. A. et al. 2007 Neutron production and implosion characteristics of a deuterium gas-puff z pinch. *Phys. Plasmas* **14**(2), 022706.

Coverdale, C. A., Deeney, C., Velikovich, A. L., Davis, J., Clark, R. W., Chong, Y. K., Chittenden, J., Chantrenne, S., Ruiz, C. L. and Cooper, G. W. 2007 Deuterium gas-puff z-pinch implosions on the z accelerator. *Phys. Plasmas* **14**(5).

DeGroot, J. S., Deeney, C., Sanford, T. W. L., Spielman, R. B., Estabrook, K. G., Hammer, J. H., Ryutov, D. and Toor, A. 1997 High velocity implosions on pbfa z. *The Fourth International Conference on High Density Z-Pinches*, Vol. 409. New York: American Institute of Physics.

DeGroot, J. S., Toor, A., Goldberg, S. M. and Liberman, M. A. 1997 Growth of the Rayleigh–Taylor instability in an imploding z-pinch. *Phys. Plasmas* **4**(3), 737–747.

Failor, B. H., Sze, H., Banister, J., Levine, J. S., Qi, N., Apruzese, J. P. and Lojewski, D. Y. 2007 Magnetic Rayleigh–Taylor instability mitigation in large-diameter gas puff z-pinch implosions. *Phys. Plasmas* **15**(2), 022703–022900.

Felber, F. S. 1982 Self-similar oscillations of a z pinch. *Phys. Fluids* **25**(4), 643.

Glazyrin, I. V., Diyankov, O. V., Karlykhanov, N. G. and Koshelev, S. V. Numerical analysis of mhd instability suppression in a double gas puff. *The Fourth International Conference on High Density Z-Pinches*, Vol. 409. New York: American Institute of Physics.

Haines, M. G., Lebedev, S. V., Chittenden, J. P., Beg, F. N., Bland, S. N. and Dangor, A. E. 2000 The past, present, and future of z pinches. *Phys. Plasmas* **7**(2), 1672–1680.

Levine, J. S., Banister, J. W., Failor, B. H., Qi, N., Sze, H. M., Velikovich, A. L., Commisso, R. J., Davis, J. and Lojewski, D. 2006 Implosion dynamics and radiative characteristics of a high yield structured gas puff load. *Phys. Plasmas* **13**, 082702–1.

Matzen, M. K. 1997 Z pinches as intense x-ray sources for high-energy density physics applications. *Phys. Plasmas* **4**(5), 1519–1527.

Ney, P., Rahman, H. U., Rostoker, N. and Wessel, F. J. 2001 Staged z-pinch for controlled fusion. *Phys. Plasmas* **8**, 616.

Peterkin, R. E., Frese, M. H. and Sovinec, C. R. 1998 Transport of magnetic flux in an arbitrary coordinate ale code. *J. Comput. Physics* **140**(1), 148–171.

Qi, N., Sze, H., Failor, B. H., Banister, J., Levine, J. S., Riorden, J. C., Steen, P., Sincerney, P. and Lojewski, D. 2008 Magnetic Rayleigh–Taylor instability mitigation in large-diameter gas puff z-pinch implosions. *Phys. Plasmas* **15**(2), 022703–1–022703–9.

Rahman, H. U., Ney, P., Wessel, F. J., Fisher, A. and Rostoker, N. 1989 Thermonuclear fusion by a z-θ pinch. *Dense Z-Pinches*, Vol. 195. New York: American Institute of Physics.

Rahman, H. U., Wessel, F. J. and Rostoker, N. 1995 Staged z-pinch. *Phys. Rev. Lett.* **74**, 714.

Rahman, H. U., Ney, P., Van Drie, A., Rostoker, N. and Wessel, F. J. 2004 Control of the Rayleigh-Taylor Instability in a Staged Z-pinch. *Phys. Plasmas* **11**, 5595.

Rostoker, N. and Tahsiri, H. 1978 *Rayleigh Taylor Instability for Impulsively Accelerated Shells; A perspective of Physics* (ed. Sir Rudolph Peierls). New York: Gordon and Breech.

Ryutov, D. D., Derzon, M. S. and Matzen, M. K. 2000 The physics of fast z pinches. *Rev. Mod. Phys.* **72**, 167–224.

Shiloh, J., Fisher, A. and Rostoker, N. 1978 Z pinch of a gas jet. *Phys. Rev. Lett.* **40**, 515.

Velikovich, A. L., Cochran, F. L. and Davis, J. Suppression of Rayleigh–Taylor instability in z-pinch loads with tailored density profiles. *Phys. Rev. Lett.* **77**(5), 853–856.

Yu, E. P. et al. 2008 Three-dimensional effects in trailing mass in the wire-array z pinch. *Phys. Plasmas* **15**, 056301–1–056301–9.